IJC
International Journal of Cancer

LEF1 supports metastatic brain colonization by regulating glutathione metabolism and increasing ROS resistance in breast cancer

Raquel Blazquez[1,2*], Eva Rietkötter[2*], Britta Wenske[1,2*], Darius Wlochowitz[3], Daniela Sparrer[1], Elena Vollmer[1], Gunnar Müller[1], Julia Seegerer[1], Xueni Sun[4], Katja Dettmer[4], Alonso Barrantes-Freer[5,6], Lena Stange[7], Kirsten Utpatel[8], Annalen Bleckmann[2,9], Hannes Treiber[2,10], Hanibal Bohnenberger[11], Christof Lenz[12,13], Matthias Schulz[2], Christian Reimelt[14], Christina Hackl[15], Marian Grade[16], Deram Büyüktas[2], Laila Siam[17], Marko Balkenhol[18], Christine Stadelmann[5], Dieter Kube[2], Michael P. Krahn[19], Martin A. Proescholdt[20], Markus J. Riemenschneider[7], Matthias Evert[8], Peter J. Oefner[4], Chistoph A. Klein[14,21], Uwe K. Hanisch[5†], Claudia Binder[2] and Tobias Pukrop[1,2]

[1]Department of Internal Medicine III, Hematology and Medical Oncology, University Hospital Regensburg, Regensburg, Germany
[2]Department of Hematology and Medical Oncology, University Medical Center Göttingen, Göttingen, Germany
[3]Institute of Medical Bioinformatics, University Medical Center Göttingen, Georg August University, Göttingen, Germany
[4]Institute of Functional Genomics, University of Regensburg, Regensburg, Germany
[5]Institute of Neuropathology, University Medical Center Göttingen, Göttingen, Germany
[6]Department of Neuropathology, University Medical Center Leipzig, Leipzig, Germany
[7]Department of Neuropathology, University Hospital Regensburg, Regensburg, Germany
[8]Institute of Pathology, University of Regensburg, Regensburg, Germany
[9]Department of Medical Statistics, University Medical Center Göttingen, Göttingen, Germany
[10]Max Planck Institute of Experimental Medicine, Göttingen, Germany
[11]Institute of Pathology, University Medical Center Göttingen, Göttingen, Germany
[12]Institute of Clinical Chemistry, University Medical Center Göttingen, Göttingen, Germany
[13]Max Planck Institute for Biophysical Chemistry, Göttingen, Germany
[14]Experimental Medicine and Therapy Research, University of Regensburg, Regensburg, Germany
[15]Department of Surgery, University Hospital Regensburg, Regensburg, Germany
[16]Department of General, Visceral and Pediatric Surgery, University Medical Center Göttingen, Göttingen, Germany
[17]Department of Neurosurgery, University Medical Center Göttingen, Göttingen, Germany

*R.B., E.R. and B.W. contributed equally to this work

Additional Supporting Information may be found in the online version of this article.

Key words: brain metastasis, glutathione, LEF1, metastatic colonization, ROS

Abbreviations: ATCC: American Type Culture Collection; BSO: buthionine sulphoximine; CFA: colony formation assay; CK: cytokeratin; CNS: central nervous system; CTC: circulating tumor cell; CTL: control; CTRL: control; DCFDA: dichlorofluorescin diacetate; DEP: differential expressed protein; ECAD: E-cadherin; ECM: extracellular matrix; EMT: epithelial-mesenchymal transition; FACS: fluorescence-activated cell sorting; FCS: fetal calf serum; FFPE: formalin-fixed paraffin-embedded; GSH: glutathione; GSSG: glutathione disulfide; GTR: gross total resection; HE: hematoxylin-eosin; HR: hazard ratio; IHC: immunohistochemistry; LEF1: lymphoid enhancer-binding factor-1; MMPI: macro-metastasis/organ parenchyma interface; MTT: methyltetrazolium; NEM: N-ethylmaleimide; NSCLC: nonsmall cell lung cancer; OS: overall survival; PBS: phosphate-buffered saline; PPI: protein–protein interaction; PWM: position weight matrix; Px: pixel; qRT-PCR: quantitative real-time PCR; ROS: reactive oxygen species; RT: reverse transcription; SD: standard deviation; SDS: sodium dodecyl sulfate; SILAC: stable isotope labeling by amino acids in cell culture; TBHP: tert-butyl hydroperoxide; TCF: T-cell factor; TF: transcription factor; TSS: transcription start site; VIM: vimentin; WHO: World Health Organization; XDH: xanthine dehydrogenase; YAP: yes-associated protein

Conflict of interest: The authors declare that they have no competing interests.

† U.K.H. passed away during the manuscript writing process

Grant sponsor: Bundesministerium für Bildung und Forschung; **Grant number:** 0316173C; **Grant sponsor:** Deutsche Forschungsgemeinschaft; **Grant number:** PU 355/5-1; **Grant sponsor:** European Union Interreg V program; **Grant number:** BY-CZ-118

DOI: 10.1002/ijc.32742

History: Received 18 Mar 2019; Accepted 30 Sep 2019; Online 18 Oct 2019

Correspondence to: Prof. Dr Tobias Pukrop, E-mail: tobias.pukrop@ukr.de

[18]Comprehensive Cancer Center, University Medical Center Göttingen, Göttingen, Germany
[19]Internal Medicine D, University Hospital Münster, Münster, Germany
[20]Department of Neurosurgery, University Hospital Regensburg, Regensburg, Germany
[21]Project Group "Personalized Tumour Therapy", Fraunhofer Institute for Toxicology and Experimental Medicine, Regensburg, Germany

More than half of all brain metastases show infiltrating rather than displacing growth at the macro-metastasis/organ parenchyma interface (MMPI), a finding associated with shorter survival. The lymphoid enhancer-binding factor-1 (LEF1) is an epithelial-mesenchymal transition (EMT) transcription factor that is commonly overexpressed in brain-colonizing cancer cells. Here, we overexpressed LEF1 in an *in vivo* breast cancer brain colonization model. It shortened survival, albeit without engaging EMT at the MMPI. By differential proteome analysis, we identified a novel function of LEF1 as a regulator of the glutathione (GSH) system, the principal cellular redox buffer. LEF1 overexpression also conferred resistance against therapeutic GSH depletion during brain colonization and improved management of intracellular ROS. We conclude that besides EMT, LEF1 facilitates metastasis by improving the antioxidative capacity of epithelial breast cancer cells, in particular during colonization of the brain parenchyma.

What's new?

More than half of all brain metastases show infiltrating rather than displacing growth at the macro-metastasis/organ parenchyma interface (MMPI), a finding associated with shorter survival. LEF1 is an epithelial-mesenchymal transition (EMT) transcription factor commonly overexpressed in brain-colonizing breast cancer cells. Its role in infiltrative MMPIs remains unclear, however. This study identifies LEF1 as a critical regulator of glutathione metabolism aside from its EMT inducer role. LEF1 overexpression induces resistance against glutathione depletion and improves the antioxidative capacity of breast cancer cells. Increased glutathione fitness and reactive oxygen species resistance appear to be more relevant than EMT induction during brain colonization.

Introduction

About 8% of patients with metastatic breast cancer will develop brain metastases with an estimated median overall survival (OS) of 11 months. This is the worst OS compared to all other sites of metastasis, such as liver, lung or bone with an estimated OS of 19, 20 and 31 months, respectively.[1] Due to improved tumor control outside of the CNS,[2] the brain has become increasingly the first site of relapse and brain metastases the final cause of death.

Until recently, neurosurgeons assumed that, contrary to WHO IV malignant brain tumors, brain metastases grow only by displacing but not by infiltrating the adjacent brain parenchyma beyond the glial pseudo-capsule. For this reason, brain metastases have been conventionally resected to the pseudocapsule (gross total resection = GTR). However, retrospective autopsy studies revealed that approximately 60% of brain metastases infiltrated the adjacent brain parenchyma.[3–5] In a prospective clinical basket trial, we found recently the 2-year OS of patients with noninfiltrative metastases to be 43.5%, while that of patients with brain metastases displaying infiltrative growth was only 6.6%. Infiltrative growth also carried a significant hazard ratio (HR) of 3.3 ($p = 0.0097$) as opposed to typical clinical parameters.[6] These and other results[7] led to a change in clinical neurosurgical practice from GTR toward a supra-marginal resection of noneloquent brain metastases.[8]

To date, three different major growth patterns have been described at the macro-metastasis/organ parenchyma interface (MMPI): displacing, epithelial infiltrative and diffuse infiltrative. A single macro-metastasis is initially not lethal but its further dissemination in the organ usually results in organ destruction and death. Consequently, the prevention of infiltration at the MMPI will at least slow down metastatic progression and prolong survival. Unfortunately, our understanding of metastatic infiltration is at best circumstantial, with current concepts arising mostly from studies of primary tumors. These concepts suggest that, comparable to invasion in the primary tumor, epithelial-mesenchymal transition (EMT) may play a major role at the epithelial infiltrative MMPI.

In lung cancer, one of the few factors reported to influence metastatic colonization[9] and survival of patients with brain metastasis[10] is the lymphoid enhancer-binding factor-1 (LEF1). Interestingly, LEF1 is also one of the few commonly overexpressed genes in different brain-seeking breast cancer cells.[11] LEF1 is a member of the T-cell factor (TCF)/LEF1 family of high-mobility group transcription factors.[12] It is a downstream mediator of the Wnt/β-catenin signaling pathway, but it can also modulate gene transcription independently.[13] LEF1 plays an essential role in EMT by activating the transcription of hallmark EMT effectors like N-cadherin, vimentin, and snail.[14,15] Thus, we hypothesized that LEF1 induces EMT at epithelial infiltrative MMPIs of breast cancer cells in the brain with the consequence of faster organ destruction and shorter OS.

Materials and Methods

Cell lines and stable transfection

Cell lines (4T1 [RRID:CVCL_0125], 410.4 [RRID:CVCL_W343]) were purchased from the American Type Culture Collection

(ATCC) and cultured in Dulbecco's Modified Eagle's Medium (DMEM) with 10% FCS (Invitrogen, Carlsbad, CA) at 37°C in a humidified 5% CO_2 atmosphere. All experiments were performed with mycoplasma-free cells. If not indicated otherwise, all substances were purchased from Sigma. Cells (410.4) were stably transfected with the pIRES2-EGFP vector (Clontech, Mountain View, CA) containing the human *LEF1* gene using the Nanofectin kit (PAA) in accordance with the manufacturer's protocol. Selection was performed by using Geneticin® resistance (G418, Roche).

RNA isolation, reverse transcription and qRT-PCR

RNA from cell lines was isolated using the High Pure RNA isolation kit (Roche) in accordance with the manufacturer's protocol. RNA from fresh-frozen mice tissue was isolated by a modified TRIzol® (Invitrogen) method incorporating a DNase I (Roche) digestion step. Reverse transcription (RT) was performed with the iScript Master Mix (BioRad, Hercules, CA). Quantitative RT-PCR (qRT-PCR) was performed as previously described[16] on an ABI Prism 7,900 HT system using mRNA specific intron-spanning primers (Supporting Information Table S1) and the SDS Software Version 2.4 (Applied Biosystems, Foster City, CA) for data analysis.

Protein extraction and Western blotting

Total protein was extracted using RIPA lysis buffer (150 mM NaCl, 0.1% SDS, 0.5% sodium deoxycholate, 1% Triton X-100, 50 mM Tris, pH 7.2). Protein extracts (20–30 µg) were subjected to SDS-PAGE and blotted onto a nitrocellulose membrane (Amersham Biosciences, Little Chalfont, UK). Membranes were incubated with specific antibodies (Supporting Information Table S2). Signals were detected with ECL Prime (Amersham Biosciences) or Signal Fire™ ECL Reagent (Cell Signaling) using the ImageQuant LAS-4000 Mini (GE Healthcare, Chicago, IL).

ECM-based migration assay

Migration assays were performed as previously described.[17] Briefly, 5×10^5 cells were seeded on a cover slip coated with ECM. After 24 hr, the cover slip was turned over onto a six-well plate coated with ECM and the distance of migrated cells was documented after 24 hr (start) and 96 hr (end) using the EVOS™ FL microscope (Thermo Fisher Scientific, Waltham, MA). Migration speed (µm/day) was calculated using the ImageJ Software (1.49v).

Micro-invasion assay

Cell invasion was measured in a modified Boyden chamber as previously described.[18] Briefly, 1×10^5 cells were seeded in the upper wells of a modified Boyden chamber. The lower wells were filled with culture medium and the chamber was then sealed with a polycarbonate membrane (10 µm pore diameter, Pieper Filter). After 96 hr, the content of the lower chamber was collected and the tumor cells that had invaded through the membrane into the lower wells were counted using a Neubauer Counting Chamber (Blaubrand).

Intracortical syngeneic *in vivo* model

All animal work was approved by the local veterinary authorities from the Government of Lower Saxony based on European guidelines and national regulations of the German animal protection act (permission no. 55.2-2532-2-22). Experiments were performed as previously described.[19] For detailed experimental settings please refer to Supporting Information Methods.

Ethical approval

Human CNS material was obtained from the archives of the Institute of Neuropathology (Göttingen) and the Department of Neuropathology (Regensburg) in accordance with the ethical review board of the Göttingen University Medical School (ethical vote no. 24/10/05).

Histology, immunohistochemistry and scoring of brain metastases

For histological studies of human or mouse brain metastasis, tissue sections were deparaffinized, stained with hematoxylin-eosin (HE) or pretreated for immunohistochemistry (IHC) using standard techniques (see Supporting Information Table S2 and Supporting Information Methods).

For the analysis of MMPI patterns in human brain metastases, we evaluated archived histologic specimens (FFPE) of metastases excised at the Department of Neurosurgery of the Regensburg University Hospital in 2015 and 2016 and described in the neuropathological report as containing parts of adjacent non-neoplastic cerebral or cerebellar tissue ($n = 87$). As these had not been intentionally sampled to include the MMPI, most specimens featured only very small amounts of central nervous tissue and could consequently not be evaluated meaningfully for MMPI patterns. We also excluded metastases of uncommon ($n < 5$) primaries. The final cohort consisted of metastases of breast cancer ($n = 5$), nonsmall cell lung cancer ($n = 9$) and malignant melanoma ($n = 5$; see Supporting Information Table S3).

Predominant MMPI patterns were evaluated in HE and with the additional support by immunohistochemical staining, using the following criteria modified from Siam *et al*.:[6]

MMPI pattern	Predominant phenotype
Displacing	Tumor does not infiltrate surrounding brain parenchyma, no cells or cell groups detached from main tumor bulk
Epithelial infiltrative	Groups of cells that collectively infiltrate the adjacent organ parenchyma without loss of epithelial morphology and expression of epithelial markers
Diffuse infiltrative	Tumor cells with mesenchymal features that infiltrate the adjacent tissue in a chain- or swarm-like (i.e. diffuse) way
Angiotropic	Tumor cell sheaths around blood vessels (perivascular) protruding far into the adjacent tissue
Mixed	Two or more MMPI patterns are observed in the same specimen

For the analysis of LEF1 staining, the proportion of positive cells out of 300 was documented.

Proteomics (SILAC)

Breast cancer cell lines were cultured for more than six cell cycles in culture medium containing 13C6,15N2-Lys; 13C6,15N4-Arg (heavy) or unlabeled (light) amino acids in order to obtain a mass shift detectable by mass spectrometry. SILAC analysis was performed as described before.[20] For detailed experimental settings, please refer to Supporting Information Methods.

Promoter analysis

Differentially expressed proteins (DEPs) observed in both cell line comparisons were subjected to promoter analysis which comprises: (*i*) mapping of DEPs to Ensembl genes, (*ii*) extraction of corresponding promoter sequences using the geneXplain platform (v5.0; Kel A., and Wingender E., http://genexplain.com/), followed by (*iii*) the search for putative LEF1 binding sites using PWMTools v1.1.9 (Ambrosini G., PWMTools, http://ccg.vital-it.ch/pwmtools). LEF1 binding sites were searched using the position weight matrix (PWM) LEF1_MOUSE.H11MO.0.B from HOCOMOCO v11.[21] This PWM serves as a mathematical model to describe the DNA binding specificity of LEF1 in promoters. Supporting Information Figures S3*a* and S3*b* contains the PWM model for LEF1 and a sequence logo reflecting the nucleotide-specific weights of this PWM.

Promoter sequences were defined as the −700/+300 bp sequence regions with respect to their annotated transcription start sites (TSSs)[22] and retrieved in FASTA sequence format using the geneXplain platform. The PWMTools were used to scan the PWM against the promoter sequences and to compute scores for any DNA sequence of length 14 within a promoter sequence by adding up the nucleotide-specific weights at respective positions of the motif.[23] The best single match score within a promoter was determined as well as a corresponding *p*-value. The promoters were then ranked according to their *p*-values, whereby only promoters with best match scores that were associated with a *p*-value ≤0.0001 (low score cut-off in PWMTools) were considered potential LEF1 targets.

Protein–protein interaction network analysis

To investigate the functional interactions between DEPs, the web tool NetworkAnalyst v3.0 (http://www.networkanalyst.ca/)[24,25] was used to analyze protein–protein interaction (PPI) networks. The STRING[26] PPI database was selected to construct the networks using only those DEPs as an input whose corresponding gene was previously identified as a potential target of LEF1 (see section promoter analysis). The PPI network construction was used to reveal proteins, which cluster together in larger modules, and thus, are likely to function together in common pathways. Furthermore, STRING rates each PPI interaction with scores ranging from medium (400) to high (1,000) confidence. In the current study, only PPI interactions with a confidence score of at least 900 were considered for network construction. After network construction, the Module Explorer function within the NetworkAnalyst web interface was used to find significant modules ($p \leq 0.05$) by applying the WalkTrap algorithm.[25]

NetworkAnalyst's Function Explorer was used to perform a KEGG pathway analysis in order to find significant metabolic pathways ($p \leq 0.05$) for each of the modules. Finally, the PPI network was visualized using the software environment of Cytoscape v3.7.1.[27]

MTT

Cell cytotoxicity was analyzed by measurement of 2,3-diphenyl-5-methyltetrazolium chloride (MTT) conversion according to standard procedures. Briefly, 5×10^4 cells were seeded in a MW24 plate and let become adherent overnight. On the next day, they were treated with BSO for 48 hr and then incubated with 0.5 mg/ml MTT for 4 hr at 37°C. Subsequently, cells were lysed and optical density was measured at 550 nm. Cell survival was calculated as percent of the control.

GSH/GSSG measurement

First, 5×10^5 cells were seeded in a MW6 plate and let become adherent overnight. On the next day, they were pretreated with PBS (CTL) or 2.5 μM BSO for 6 hr, washed ($t = 0$ hr) and incubated without BSO for up to 24 hr. For analysis of GSSG and GSH, medium was discarded and cells were washed twice 1 min each with 1 ml PBS containing 1 mM N-ethylmaleimide (NEM, Sigma). After the addition of 10 μl of 25 μM glutathione-disulfide-(glycine-$^{13}C_4$,$^{15}N_2$) (Toronto Research Chemicals, Toronto, ON, Canada) as internal standard, cells were scrapped in 600 μl of cold 80% methanol. The extract was transferred to a 1.5-ml cup and the wells were washed once more with 400 μl of cold 80% methanol. The cell extracts were combined and centrifuged at 4°C and 10,000*g* for 5 min. The supernatant was then collected and the pellets were washed twice with 200 μl of 80% methanol. The combined supernatants were evaporated to dryness and then re-dissolved in 50 μl of water.

Determination of GSH and GSSG was performed using a Maxis Impact QTOFMS (Bruker Daltonics, Bremen, Germany) with an ESI source coupled to a Dionex Ultimate 3000 UHPLC system (Thermo Scientific) with a Diode Array Detector (Thermo Scientific, Idstein, Germany). For detailed instrumental settings, please refer to Supporting Information Methods.

Intracellular ROS measurement

Intracellular ROS was measured using the DCFDA/H2DCFDA ROS assay (Abcam) following manufacturer's instructions. Briefly, 5×10^5 cells were stained with 2′,7′ –dichlorofluorescin diacetate (DCFDA, 20 μM) for 30 min at 37°C. Next, cells were treated with tert-butyl hydroperoxide (TBHP, 200 μM) or left untreated (naïve) for 1 and 4 hr, respectively, and fluorescence (485/535 nm) was measured using a Becton Dickinson FACS Calibur flow cytometer and Cell Quest Software (BD). Intracellular ROS was determined as the difference between TBHP-treated and control (naïve) cells after background subtraction (unstained).

Anchorage-independent growth

First, 5×10^5 cells were seeded in a MW6 plate and let become adherent overnight. On the next day, they were pretreated with PBS (CTL) or 2.5 μM BSO for 6 hr. To analyze anchorage-independent growth, single cells were embedded in a semi-solid culture medium consisting of a bottom layer (0.5% agarose) and a top layer (0.3% agarose), in which the cells were embedded. Growth medium supplemented with 2.5 μM BSO or PBS was added to the corresponding wells and replaced every other day. Cell cultures were incubated for up to 3 weeks and analyzed using an Axio Observer Z1 microscope (Zeiss) and the VisiView Imaging Software (Visitron Systems GmbH).

Statistics

Unless indicated otherwise, all values were expressed as means ± standard deviation (SD). Statistical differences were analyzed by Student's *t*-test, one-way ANOVA or log-rank test using GraphPad Prism software version 8 (GraphPad, San Diego, CA). $p < 0.05$ was considered significant.

Data availability

The data that support the findings of our study are available on request from the corresponding author. The data are not publicly available due to privacy or ethical restrictions.

Results

Brain metastases show different MMPI patterns

Since our previous publication had hinted at entity-specific MMPI patterns,[6] we retrospectively assessed a cohort of resected cerebral and cerebellar metastases with evaluable adjacent brain tissue (n = 20). In this cohort, a displacing (noninfiltrative) growth behavior was exclusively seen in a single available specimen of renal cell carcinoma. All other brain metastases infiltrated the adjacent brain parenchyma (19/20), albeit with distinctive MMPI patterns (Fig. 1 and Supporting Information Table S3). In brain metastases from breast cancer patients (n = 5), we observed in 3/5 cases predominantly an epithelial infiltrative MMPI. The other two cases showed either purely diffuse infiltration of the adjacent brain parenchyma or a combination of epithelial and diffuse infiltration (mixed MMPI). In non-small cell lung cancer (NSCLC) brain metastases (n = 9), in contrast, we observed roughly equal fractions of epithelial (3/9), diffuse (2/9) and mixed (4/9) infiltration. All five cases of malignant melanoma featured diffuse cancer cell infiltration. In addition, 2/5 melanoma specimens showed angiotropic infiltration into the brain parenchyma along preexisting blood vessels.[6] Thus, we confirmed our previous observation of distinct infiltration patterns of brain metastases and the apparently preferential epithelial infiltration pattern of breast cancer brain metastases.[6]

LEF1 supports CNS colonization in a breast cancer syngeneic model

In order to investigate the role of LEF1 in typical breast cancer brain metastases, we first searched for suitable *in vivo* models that reflect the epithelial MMPI pattern. Given that the resident organ defense, consisting of microglia and astrocytes, assists the infiltration of breast cancer cells[17,19,28–30] and that oncogenic activation of β-catenin or LEF/TCF is linked to T cell immunity,[31] we favored syngeneic over xenograft models. We chose the murine breast cancer cell line 4T1 and its less aggressive parental cell line 410.4.[32] First, we confirmed that both cell lines infiltrated the brain parenchyma beyond the glial pseudo-capsule and displayed overall the same epithelial MMPI pattern typical of breast cancer (Fig. 2*a*). Furthermore, mice with intracortically injected 4T1 cells developed symptomatic macro-metastases within a median of 19 days, while the respective median in mice injected with 410.4 was 70.5 days ($p \leq 0.001$; Fig. 2*b*). Interestingly, in accordance with previous xenograft results of brain-seeking breast cancer cells and their respective parental clones,[11] the significantly better colonizing 4T1 revealed a higher *LEF1* expression (Fig. 2*c*). Moreover, *in vitro* the mesenchymal and EMT marker vimentin was only observed in 4T1 cells, while E-cadherin was strongly expressed in 410.4 (Fig. 2*d*). The 410.4 cells were also significantly less invasive than the 4T1 cells *in vitro* ($p \leq 0.001$; Fig. 2*e*). However, expression of *Axin2*, the typical target gene of WNT/β-catenin-signaling, did not differ between 410.4 and 4T1 cells (Fig. 2*f*), indicating that LEF1 probably functions in a WNT/β-catenin independent fashion as recently described.[13] Both cell lines expressed similar levels of the epithelial intermediate filament cytokeratin 8 (CK8) (Fig. 2*d*). They displayed *in vitro* an epithelial growth pattern, with the 410.4 cells growing in tight clusters, while the 4T1 were more loosely packed and displayed some mesenchymal features (Fig. 2*g*).

To further investigate the role of LEF1, we overexpressed it in the moderately metastatic and less invasive 410.4 cells. Surprisingly, LEF1 overexpression had no evident impact on the epithelial features of 410.4 cells *in vitro* (Figs. 3*a* and 3*b*) and significantly decreased the migration and invasion capacity of these cells (Figs. 3*c* and 3*d*). Nevertheless, LEF1 overexpression significantly improved the colonization capacity of the 410.4 cells *in vivo* and led to a shortened OS (median OS = 53 days) compared to the 70.5 days of the control group (EGFP; p = 0.02; Fig. 3*e*). Additionally, overexpression of *LEF1* neither stabilized β-catenin nor affected the expression of *Axin2* and the epithelial markers *Ck8* and *Ecad* in 410.4 metastatic tissues (Fig. 3*f*). Again, both findings underline the WNT/β-catenin independent effects of LEF1. Despite the missing induction of EMT *in vitro*, we searched nevertheless *in vivo* for signs of EMT, especially at the MMPI. Thus, we first analyzed the expression of E-cadherin in all brain metastasis mouse models. Unexpectedly, we noticed often an upregulation of E-cadherin at the epithelial infiltrating MMPIs and in the locally disseminated micro-metastases regardless of the cell line even when the metastatic core was E-cadherin

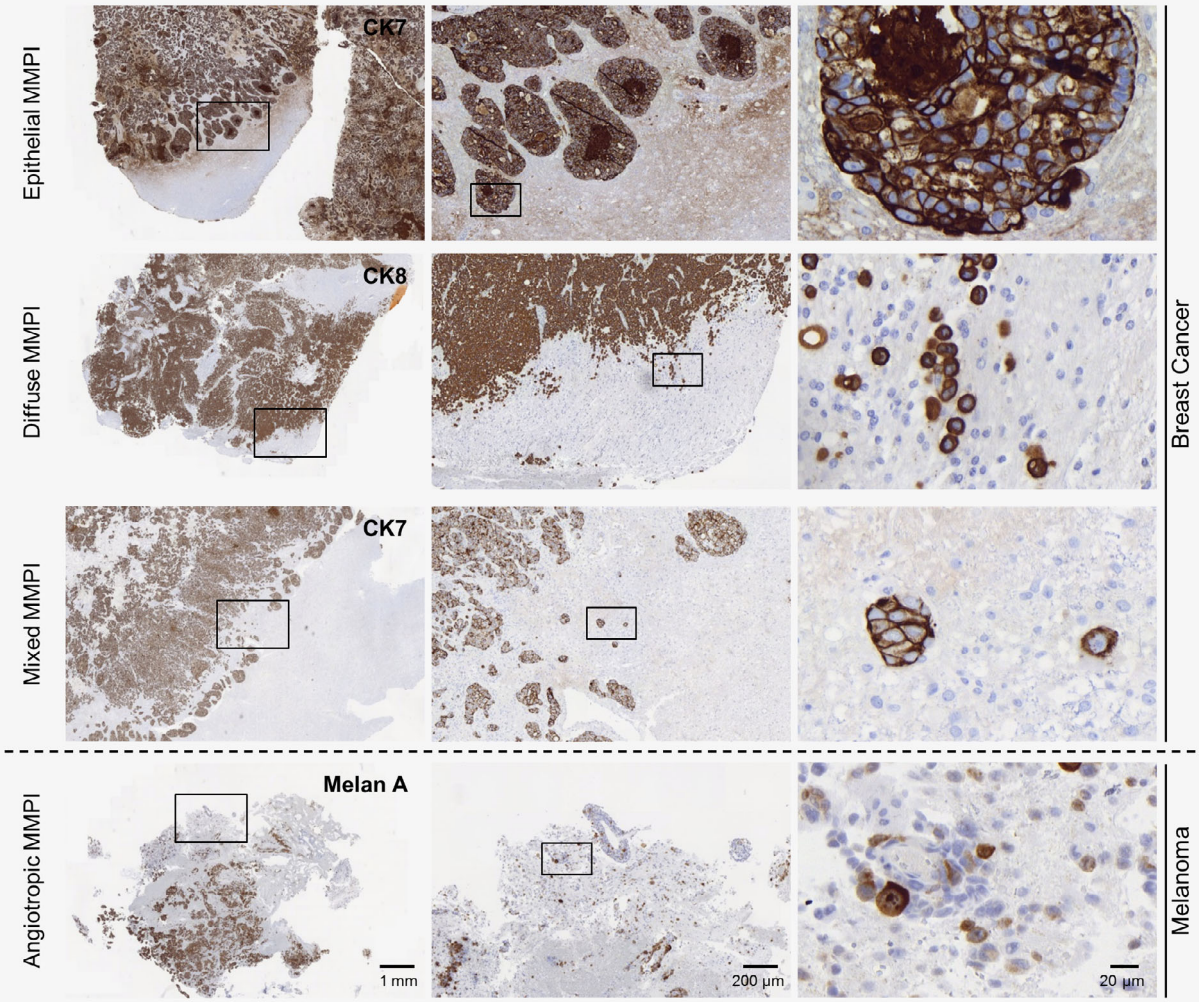

Figure 1. MMPI patterns of human brain metastases. Cytokeratin 7 (CK7), cytokeratin 8 (CK8) and Melan A staining in tissue sections of human cerebral metastases. Representative images of epithelial (first row), diffuse (second row) and mixed (epithelial and diffuse, third row) infiltration at the MMPI of breast cancer brain metastases; the fourth row shows angiotropic infiltration in a melanoma brain metastasis. [Color figure can be viewed at wileyonlinelibrary.com]

negative or necrotic (Fig. 3*g*). Additionally, semi-thin sections of the more mesenchymal and vimentin-expressing 4T1 brain metastases showed infiltrating 4T1 clusters (Supporting Information Fig. S1*a1*), which presented electro-dense contacts between the infiltrating carcinoma cells *in vivo* as revealed by electron microscopy (EM; Supporting Information Fig. S1*a*2–S1*a*3). Thus, all cell lines, including the highly vimentin-expressing 4T1 cells, showed an epithelial infiltrating MMPI pattern with dense cell–cell contacts, but without signs of EMT. Even the overexpression of the EMT-inducer LEF1 did not cause EMT-like changes.

Intact contact inhibition

The upregulation of E-cadherin indicated epithelial barrier formation and intact contact inhibition at the metastatic margins. Thus, we investigated whether the tested breast cancer cells upregulated p-YAP with increasing cell density as a marker for intact contact inhibition. Indeed, in all cell types, including 4T1, p-YAP increased with confluence, while the expression of YAP remained constant. Moreover, the expression of E-cadherin and β-catenin increased also with confluence (Supporting Information Figs. S1*b* and S1*c*). These results demonstrate that the tested epithelial breast cancer cells retain their contact inhibition capacity.

Cell clusters and E-cadherin expression at the MMPI of human brain metastases

Having shown that LEF1 supports metastatic brain colonization in a murine breast cancer model, we investigated next whether LEF1 was also expressed in human breast cancer brain metastases. For this, we analyzed the expression of LEF1

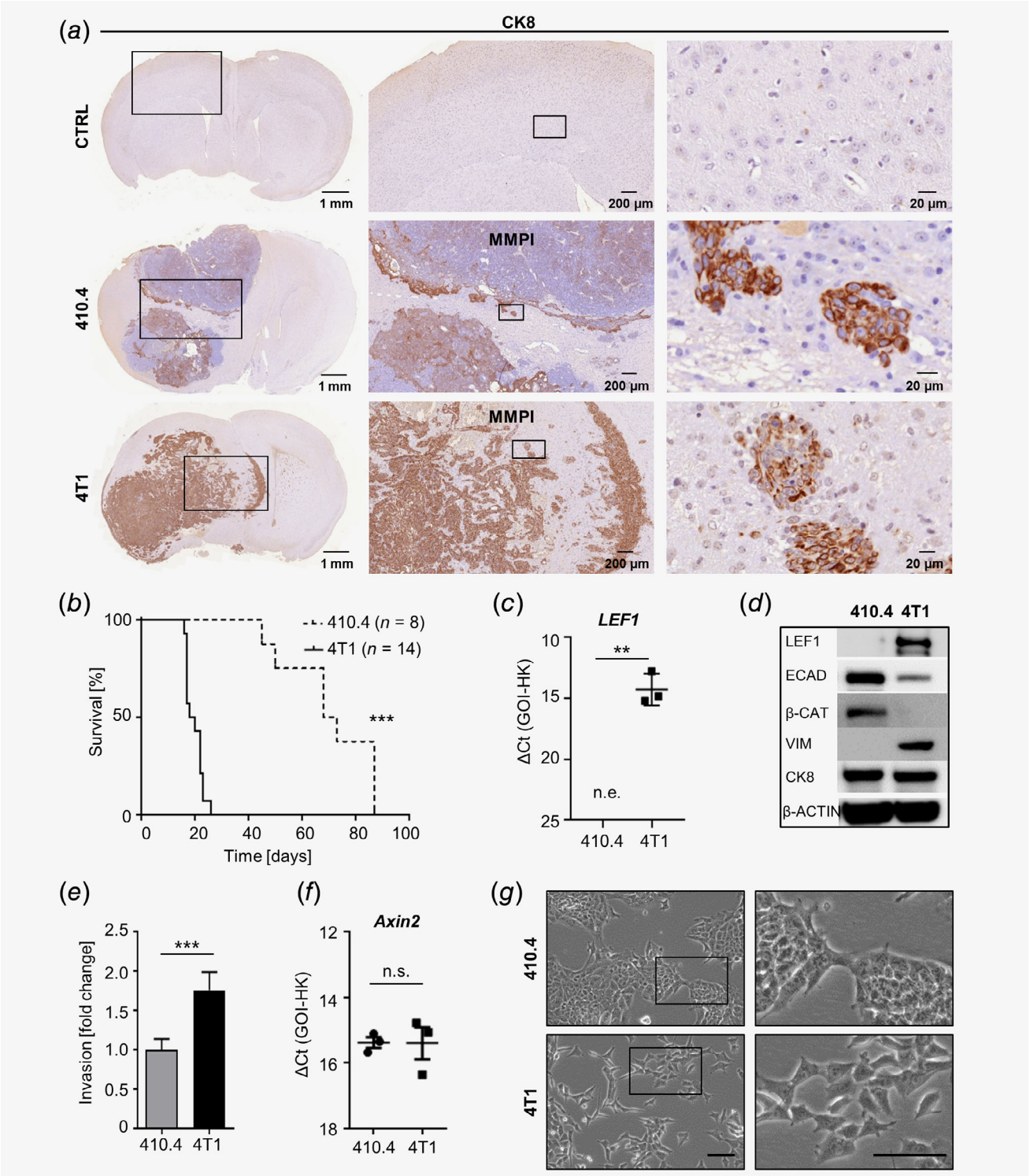

Figure 2. Characterization of LEF1 expression in murine breast cancer cells. (*a*) Cytokeratin 8 (CK8) staining in tissue sections of 410.4 and 4T1 breast cancer brain metastases, respectively. A section of a mouse injected without tumor cells is shown as a control (CTRL). Images of the MMPI at higher magnification are also shown. (*b*) Kaplan-Meier survival curves of mice injected with 410.4 ($n = 8$) or 4T1 ($n = 14$; log-rank test; ***$p \leq 0.001$). (*c*) Quantitative RT-PCR analysis of *LEF1* expression in 410.4 and 4T1 (squares; $n = 3$; *t*-test; **$p \leq 0.01$; n.e. = not expressed). (*d*) Western blot analysis of the indicated proteins in 410.4 and 4T1. One representative loading control is shown. (*e*) Micro-invasion assay. The invasiveness of 4T1 is indicated as fold change relative to 410.4 ($n = 8$; *t*-test; ***$p \leq 0.001$). (*f*) Quantitative RT-PCR analysis of *Axin2* in 410.4 (circles) and 4T1 (squares; $n = 3$; *t*-test; n.s. = not significant). (*g*) Phase-contrast images of 410.4 and 4T1. Scale bars = 100 µm. [Color figure can be viewed at wileyonlinelibrary.com]

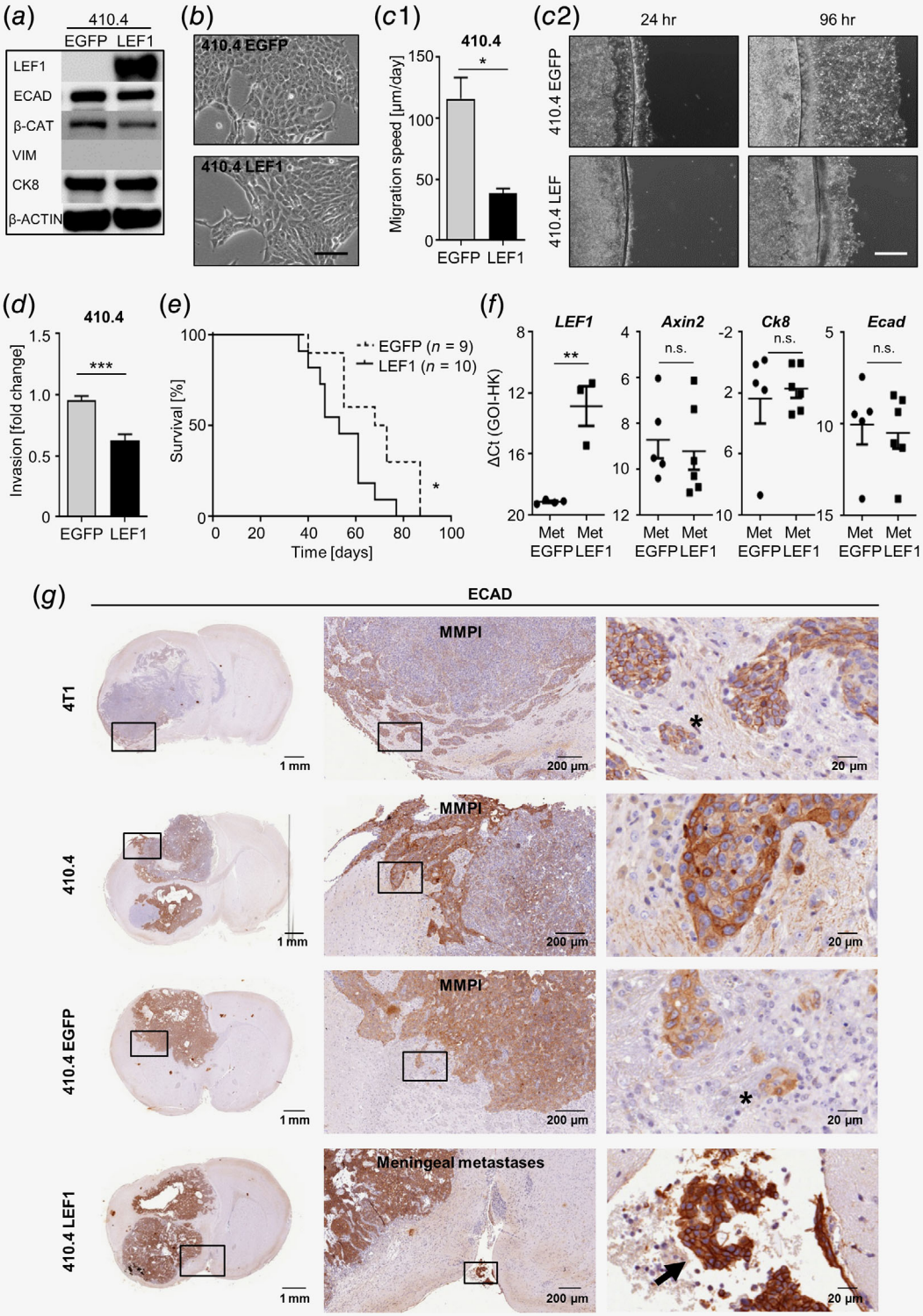

Figure 3. LEF1 overexpression in 410.4 breast cancer cells. (*a*) Western blot analysis of the indicated proteins in 410.4 stable transfected with the empty vector (EGFP) or LEF1. One representative loading control is shown. (*b*) Phase contrast images of 410.4 control (EGFP) or LEF1-overexpressing (LEF1) cells. Scale bars = 100 µm. (*c*) ECM-based migration assay. (*c*1) Migration speed is indicated as µm/day ($n = 2$; *t*-test; $^{*}p \leq 0.05$) and (*c*2) representative images are shown. Scale bars = 500 µm. (*d*) Modified Boyden chamber invasion assay. The invasiveness of 410.4 LEF1 is indicated as fold change relative to 410.4 EGFP ($n = 3$; *t*-test; $^{***}p \leq 0.001$). (*e*) Kaplan-Meier survival curves of mice injected with 410.4 EGFP ($n = 9$) or LEF1 ($n = 10$; log-rank test; $^{*}p \leq 0.05$). (*f*) Quantitative RT-PCR analysis of the indicated genes in brain metastases of 410.4 EGFP or LEF1 ($n \geq 3$; *t*-test; $^{**}p \leq 0.01$, n.s. = not significant). (*g*) E-cadherin (ECAD) IHC staining in tissue sections of 4T1, 410.4, 410.4 EGFP and 410.4 LEF1. Representative images of the MMPI and meningeal metastases are shown. Locally disseminated micro-metastases are indicated with asterisks; meningeal metastases with an arrow. [Color figure can be viewed at wileyonlinelibrary.com]

in a retrospective cohort of GTR resected breast cancer human brain metastases. In 87.1% of the specimens (n = 27/31), we detected varying nuclear LEF1 expression in the bulk of the metastatic tissue; the proportion of LEF1 positive nuclei ranged from 1% to 55% (Fig. 4*a*). Hence, LEF1 is expressed in the majority of breast cancer cerebral metastases during colonization of the brain parenchyma.

To verify missing signs of EMT at the MMPI in human epithelial brain metastases, we evaluated in analogy to the *in vivo* models the expression of E-cadherin and vimentin in the above

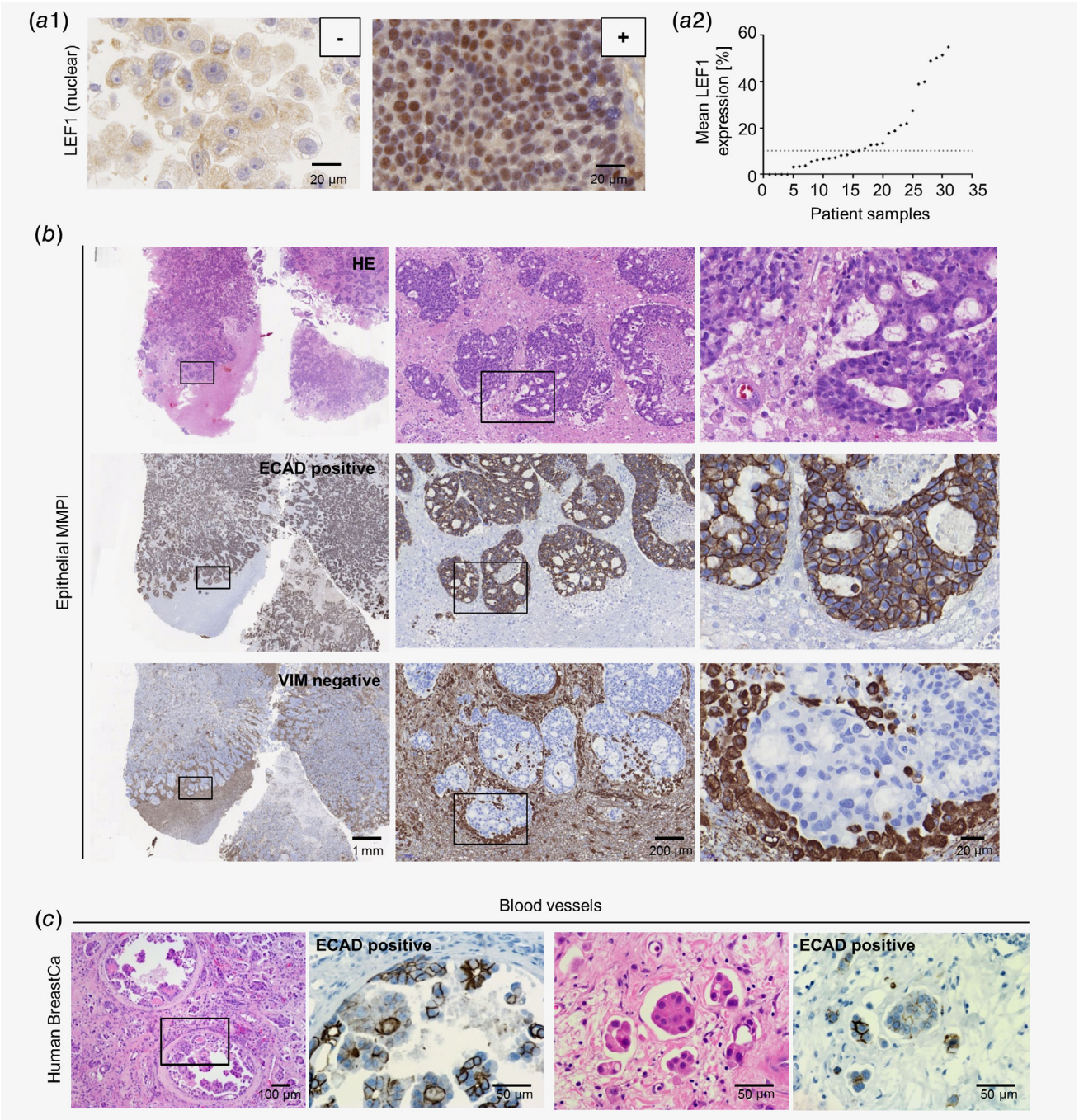

Figure 4. LEF1, E-cadherin and vimentin expression in human brain metastases. (*a*1) Breast cancer brain metastases that are either negative (–) or positive (+) for nuclear LEF1 IHC staining in 1–55% of tumor cells. (*a*2) Distribution of mean nuclear LEF1 expression for each of the 31 brain metastases analyzed by IHC. Dotted line indicates the median value. (*b*) Histology (hematoxylin-eosin, HE) and E-cadherin (ECAD) and vimentin (VIM) staining on tissue sections of epithelial infiltrating breast cancer brain metastases. (*c*) Intravascular E-cadherin (ECAD) positive cell clusters in breast cancer brain metastases. The marked section shows a bigger magnification of the blood vessel. [Color figure can be viewed at wileyonlinelibrary.com]

mentioned 4/5 breast cancer specimens displaying only epithelial or both epithelial and diffuse cancer cell infiltration at the MMPI (Fig. 1). Similar to our *in vivo* models, we detected positive E-cadherin and negative vimentin expression even at the epithelial infiltrating MMPIs (Fig. 4*b*). Additionally, we also searched for EMT signs in different primaries of the still available biopsy specimens of our previous prospective basket trial.[6] Surprisingly, while the displacing human renal cancer brain metastases were only positive for vimentin (Supporting Information Fig. S2*a*), the epithelial infiltrating MMPIs of breast cancer and NSCLC brain metastatic lesions expressed E-cadherin but no vimentin (Supporting Information Fig. S2*b*). Moreover, we also detected E-cadherin positive carcinoma cell clusters, analog to our *in vivo* models, in adjacent blood vessels of human breast cancer brain metastases (Fig. 4*c*). In summary, the frequent expression of LEF1 in breast cancer brain metastases suggests a prominent role during colonization, however without engaging EMT during epithelial infiltration at the MMPI.

LEF1 modulates GSH metabolism

Since the above findings had indicated an EMT- and WNT/β-catenin-independent function of LEF1, we searched for an alternative mechanism that might explain how LEF1 supported the metastatic colonization of breast cancer cells in the brain. For this, we compared the proteome of the moderately metastatic 410.4 cells with those of the highly metastatic 4T1 and the 410.4 LEF1 cells, respectively, by stable isotope labeling in cell culture (SILAC) and mass spectrometry. We found a total of $n = 122$ differentially expressed proteins (DEPs) in the first comparison (410.4 *vs*. 4T1 DEPs, Supporting Information Table S4) and $n = 65$ in the second one (410.4 *vs*. LEF1 DEPs, Supporting Information Table S5; 125 and 88 unique gene symbols, respectively). Eleven proteins (common DEPs) with 14 unique gene symbols were commonly differentially expressed in both comparisons. Remarkably, 7/11 common DEPs were related to glutathione (GSH) metabolism (Fig. 5*a*). Next, we asked which of these 11 common DEPs might be potentially regulated by LEF1 at the gene level. To that end, we used an *in silico* method to search for putative LEF1 binding sites within the promoter regions of the corresponding genes ($n = 14$) with available promoters. Only those genes/promoters with a p-value ≤0.0001 were considered significant. Our promoter analysis revealed that 6/14 genes from the common DEPs had LEF1 binding sites, namely, *Gstm1*, *Mgst1*, *Tmem209*, *Serpinb2*, *Gsta1* and *Xdh* (Supporting Information Fig. S3*c* and Table S6). Remarkably, 4/6 of these genes (*Gstm1*, *Mgst1*, *Gsta1* and *Xdh*) encode scavengers of reactive oxygen species (ROS). To confirm that LEF1 could indeed directly regulate the four genes involved in ROS elimination and GSH metabolism, we analyzed their expression in 410.4 CTRL, 410.4 LEF1 and 4T1 cells by qRT-PCR. Indeed, except for Gsta1, we observed significantly increased expression levels of *Gstm1*, *Mgst1* and *Xdh* in the 410.4 LEF1 and 4T1 cells compared to 410.4 control cells (CTRL; Fig. 5*b*). Moreover, we detected a positive expression of XDH by IHC in the 3/4 human breast cancer specimens mentioned above. In contrast, the only breast cancer specimens displaying diffuse infiltration were negative for XDH (Fig. 5*c*).

Encouraged by these findings, we finally aimed to understand the organization and functionality of the three LEF-regulated genes/DEPs *Gstm1*, *Mgst1* and *Xdh* using network-based approaches. For our analysis, we constructed a PPI network using the STRING database. The three LEF-regulated genes/DEPs (nodes) were visualized in the PPI network and their connections were established. Modular analysis of the PPI network resulted in two clusters. Both clusters were subjected to pathway enrichment analysis (KEGG database). In the first cluster, enrichment analysis identified the following pathways: chemical carcinogenesis, glutathione metabolism and metabolism of xenobiotics. The second cluster comprised caffeine metabolism, drug metabolism and purine metabolism (Fig. 5*d* and Supporting Information Table S7). Most importantly, the link between the two clusters was detoxifying metabolic systems and the amino acid glycine. Glycine is critical for GSH production and purine biosynthesis in rapidly dividing cancer cells. Glycine restriction reduced the levels of GSH synthesis and increased ROS in cancer cells *in vitro*.[33]

In order to investigate whether LEF1 increased in fact ROS resistance and GSH fitness in the breast cancer cells, we stressed the cells with the ROS inducer TBHP and measured their capacity to cope with intracellular ROS over time. Interestingly, only the cells with LEF1 overexpression (4T1 and 410.4 LEF1) maintained stable intracellular ROS levels. In the 410.4 control cells (410.4 CTRL), however, ROS levels significantly increased (Fig. 6*a*1 and *a*2). These results underline the impact of LEF1 on ROS resistance and the dynamic regulation of the ROS scavenging systems. Furthermore, to investigate the role of LEF1 in GSH synthesis, we inhibited the *de novo* synthesis of GSH by treating the murine breast cancer cells 4T1, 410.4 CTRL and 410.4 LEF1 with buthionine sulphoximine (BSO). Interestingly, the 410.4 control cells had the highest sensitivity to BSO, while the LEF1 expressing cell lines (4T1 and 410.4 LEF1) showed higher inhibitory coefficients (Fig. 6*b*). Most importantly, 24 hr after BSO removal, the 410.4 LEF1 and 4T1 cells recovered their glutathione redox status, while the GSH/GSSG ratio of the 410.4 was still reduced to less than 30% compared to the untreated cells (CTL) (Fig. 6*c*). Finally, to investigate whether metabolic GSH fitness influenced the colonization capacity of the breast cancer cells, we performed colony formation assays (CFAs) under BSO treatment. Consistent with our previous results (Figs. 6*a*–6*c*), the LEF1 expressing cell lines (4T1 and 410.4 LEF1) were not impaired in their ability to form 3D colonies under BSO treatment, while the control 410.4 revealed a significantly reduced colony formation capacity (Fig. 6*d*).

In summary, our results demonstrate that LEF1 appears to confer a survival advantage to brain colonizing epithelial

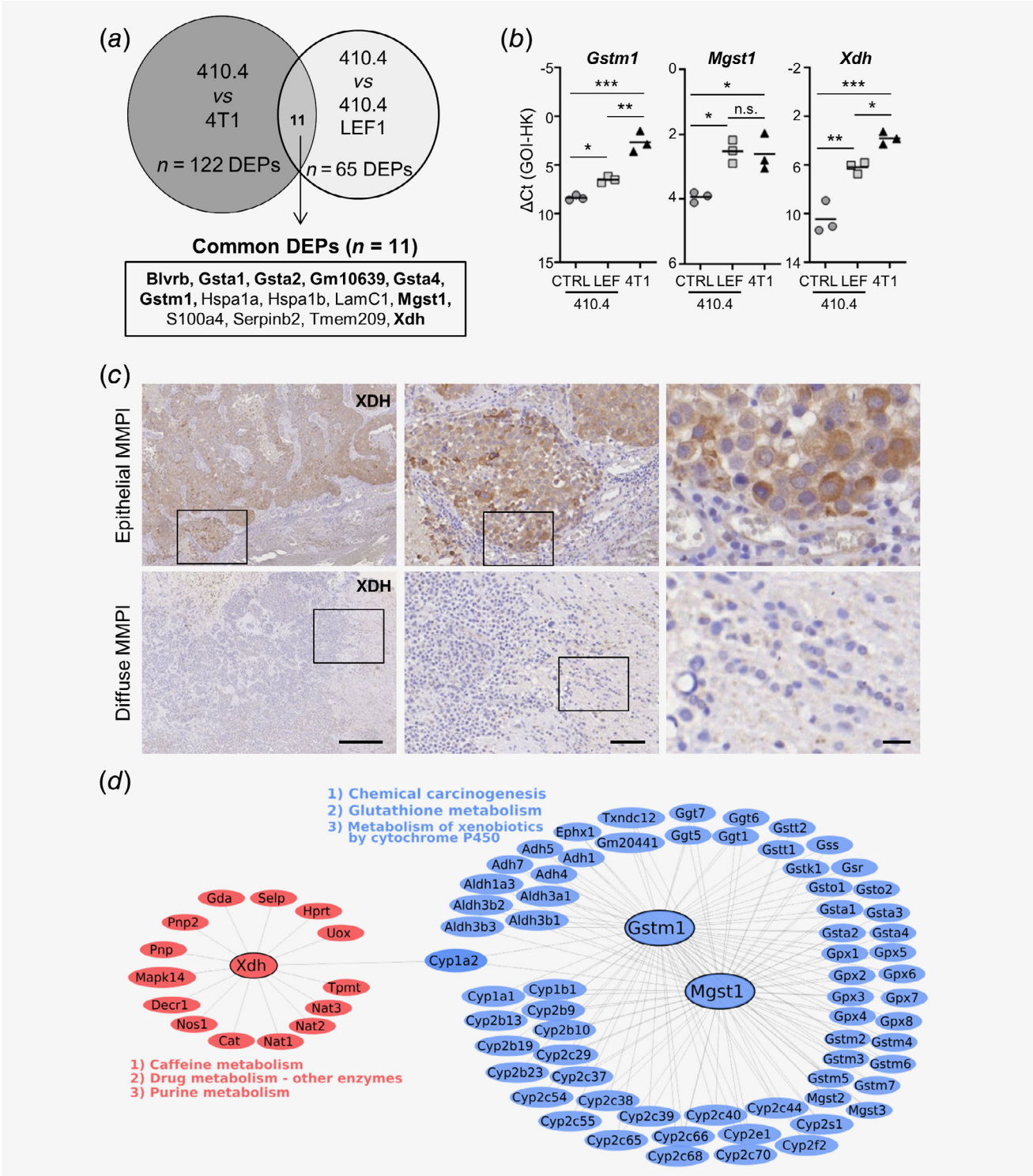

Figure 5. *In silico* screening for LEF1 target gene discovery and functional association analysis. (*a*) Venn diagram depicting the overlap (common DEPs) of differentially expressed proteins identified by proteomic comparisons between 410.4 cells with 4T1 (dark gray) and 410.4 LEF1 cells (light gray). (*b*) Quantitative RT-PCR analysis of the indicated genes in 410.4 CTRL, 410.4 LEF1 and 4T1 ($n = 3$; one-way ANOVA followed by Sidak's multiple comparisons; ***$p \leq 0.001$, **$p \leq 0.01$, *$p \leq 0.05$, n.s. = not significant). (*c*) Xanthine dehydrogenase (XDH) staining on tissue sections of epithelial (upper row) and diffuse (lower row) infiltrating breast cancer brain metastases. (*d*) Protein–protein interaction (PPI) network revolving around Xdh, Mgst1 and Gstm1. The PPI network comprises 83 proteins (nodes) and 148 interactions (edges) between proteins derived from both experimental data as well as predictions using the STRING Interactome. The node colors blue and red indicate distinct assignments to functional modules in the PPI network. The top three KEGG pathways significantly enriched in the modules are indicated with matching colors in blue and red, respectively. [Color figure can be viewed at wileyonlinelibrary.com]

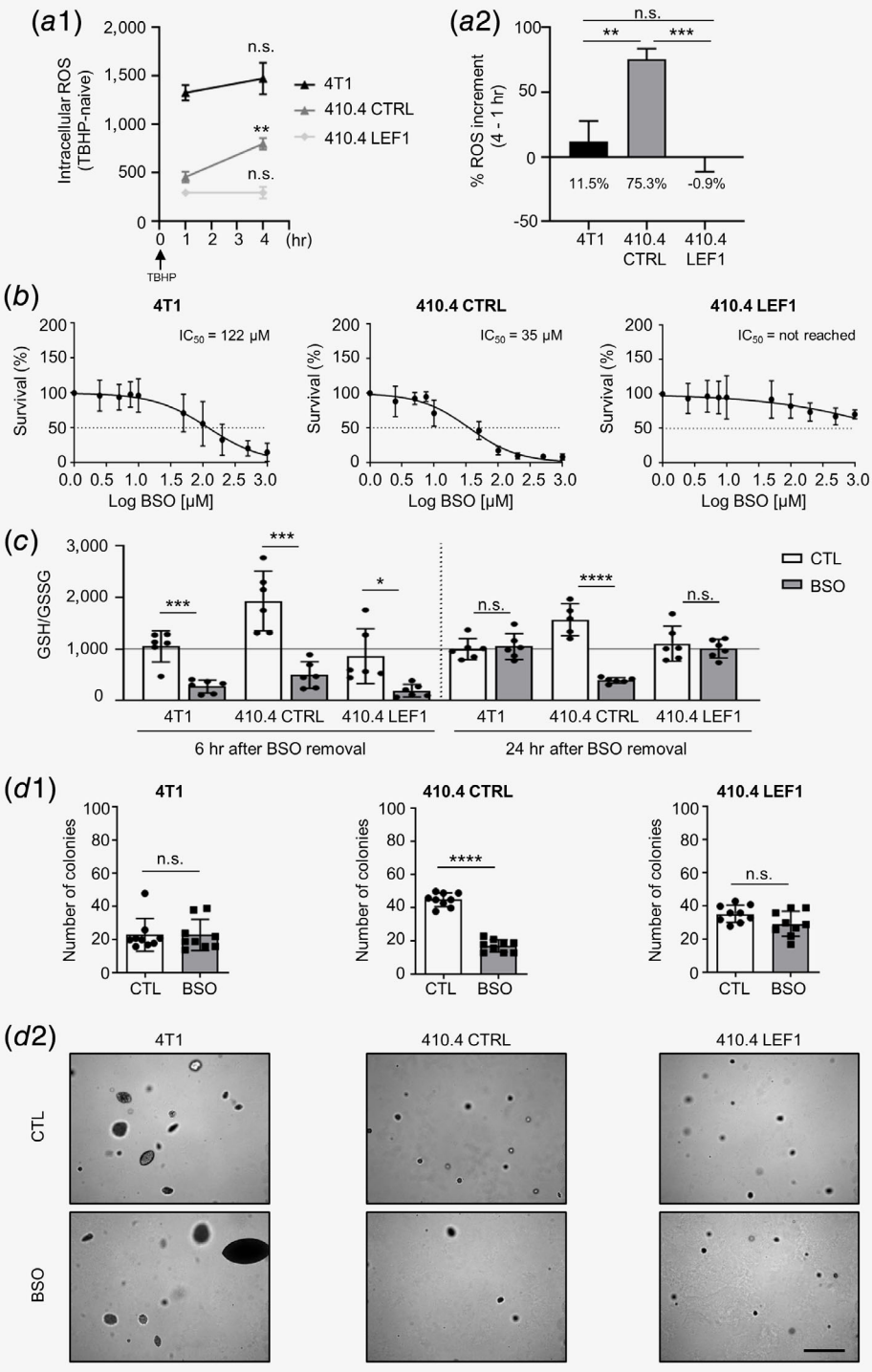

Figure 6. Regulation of GSH metabolism by LEF1. (*a*) Intracellular ROS generation. Cells were labeled with DCFDA (20 µM) or unlabeled (unstained) and then cultured for an additional 1 and 4 hr with or without 200 µM tertbutyl hydrogen peroxide (TBHP) according to the protocol. Cells were then analyzed by fluorescence-activated cell sorting (FACS). (*a1*) Intracellular ROS generation over time ($n \geq 3$; *t*-test; $^{**}p \leq 0.01$, n.s. = not significant) and (*a2*) ROS increment ($n \geq 3$; one-way ANOVA followed by Sidak's multiple comparisons; $^{***}p \leq 0.001$, $^{**}p \leq 0.01$, n.s. = not significant) are indicated. (*b*) MTT standard curves showing cell survival after 48 hr BSO treatment at the indicated concentrations. The dotted line shows the IC_{50}. (*c*) GSH/GSSG ratio measured at 6 and 24 hr after BSO removal. Cells were pretreated with PBS (CTL, white bars) or 2.5 µM BSO (BSO, gray bars) for 6 hr, washed ($t = 0$ hr) and incubated without BSO during 6 and 24 hr ($n = 6$; *t*-test; $^{****}p \leq 0.0001$, $^{***}p \leq 0.001$, $^{*}p \leq 0.05$, n.s. = not significant). (*d1*) Anchorage-independent growth of indicated cells under control conditions (CTL) or after BSO pretreatment (2.5 µM) for 6 hr ($n = 9$; *t*-test; $^{****}p \leq 0.0001$, n.s. = not significant). (*d2*) Representative images of colony formation in the indicated cell lines are shown. Scale bars = 500 µm.

cancer cells by boosting GSH levels and, thus, ROS resistance. Moreover, the LEF1-induced gain in detoxification ability seems more important for *in vivo* metastatic colonization of the brain than EMT induction.

Discussion

Metastatic organ colonization is not only the most critical but also the most ineffective step of the metastatic cascade.[34–36] Clinically, it is the most relevant phase, as the majority of cancer patients with synchronous or even metachronous metastases have already accomplished all previous steps of metastasis before cancer diagnosis. Thus, to slow down or even prevent progression of colonization is the main goal of adjuvant/metastatic systemic cancer therapy. However, despite its clinical impact, colonization of various organs is the least studied process of the metastatic cascade. This step of metastasis includes initial growth in the different host organs, outgrowth to macrometastases with subsequent organ destruction and death.

During metastatic colonization of the brain, cancer cells have to deal with high intrinsic and extrinsic ROS levels. At the beginning of colonization, the intrinsic oxidative stress derives from cell proliferation itself. Moreover, proliferation of metastatic cells pushes the metastatic daughter cells away from the vasculature, which leads to a decrease in oxygen supply and induction of hypoxia and a concomitant increase in ROS production.[37] Interestingly, circulating tumor cells (CTCs) reduce production of ROS to survive by switching towards a glycolytic metabolism and decreasing their aerobic respiration rate (oxidative phosphorylation).[38] In contrast, a recent molecular profiling study of malignant melanoma specimens derived from *in vivo* models and from a patient cohort with matched extracranial and brain metastasis revealed the importance of oxidative phosphorylation in brain metastases.[39] This indicates that during colonization of the brain, CTCs have to re-activate oxidative phosphorylation despite the associated increase in ROS production. Moreover, metastatic cancer cells are exposed to additional extrinsic oxidative stress from the resident brain parenchymal cells. Microglia and astrocytes immediately surround and attack metastatic cells after seeding.[30,40] However, metastatic cells that sustain this attack successfully often hijack the organ defense to facilitate their metastatic progression. For example, in the brain, glial cells support the epithelial metastatic cells infiltrating the brain parenchyma at the MMPI.[17,28–30] However, before overtaking the brain, metastatic cells have to survive (*i*) the restart of proliferation, (*ii*) the hypoxic conditions in this harsh environment and, finally, (*iii*) the attack of the host organ. Therefore, metastatic cells need an enormous metabolic capacity and plasticity as well as a dynamic detoxification system during colonization of the brain.

The elimination of ROS seems likewise critical in other metastatic target organs. This assumption is supported by knockdown experiments of glutaredoxin 3 (*Glrx3*). Glrx3 is an oxidoreductase, which reduces a variety of substrates using glutathione as cofactor. Accordingly, knockdown of *Grx3* increased ROS levels in breast cancer cells. Nonetheless, this goes along with diminished colony formation *in vitro* and reduced metastatic colonization of the lung *in vivo*.[41] In this line, another study described that 4T1 cells have increased ROS resistance after colonization of the lung, and BSO treatment accordingly reduced the amount of lung metastases.[42] Furthermore, in a B16 melanoma model, high GSH levels were protective during the early colonization of the liver. There, high levels of GSH safeguard the melanoma cells from apoptosis induced by the extrinsic attack of the organ-resident endothelial cells of the sinusoids.[43,44] Thus, GSH fitness and ROS resistance seem essential to sustain the organ defense during (early) colonization in various metastatic target organs, not only the brain.

In line with the above mentioned findings, our results also demonstrate that during colonization of the brain these features seem even more important than migration and invasion. It is well accepted that, besides migration and invasion, EMT is associated with a complex metabolic reprogramming and chemotherapy resistance.[45] Unfortunately, the previous observations failed to distinguish between the impact of EMT-induced migration and invasion and the impact of the EMT-associated metabolic reprogramming. Nevertheless, some studies already indicated that the impact of the metabolic reprogramming and induction of chemotherapy-resistance was even more relevant than the classic EMT hallmarks migration and invasion during metastatic colonization.[46,47] Our results also point in this direction. Our KEGG-based pathway analysis of the PPI network including the LEF-regulated DEPs identified drug, GSH and cytochrome P450 metabolism as enriched pathways. Interestingly, these pathways are involved in chemotherapy resistance and ROS elimination.

So far, chemotherapy-induced resistance by LEF/TCF was described in the context of WNT/β-catenin signaling or EMT. Moreover, LEF/TCF and WNT were only described as regulators of GSH metabolism during embryonic development.[43,44] However, here we demonstrate that in breast cancer cells LEF1 regulates genes responsible for GSH metabolism and chemotherapy resistance (*Gstm1*, *Mgst1* and *Xdh*). Moreover, the strengthening of the detoxifying systems was not a byproduct of EMT. By a bioinformatics approach, we identified sequences for LEF/TCF binding in the promoters of these genes and observed their upregulation after LEF1 overexpression in the breast cancer cells 410.4. Thus, LEF1 could induce detoxifying systems directly at the promoter level without induction of EMT. Moreover, our data indicate that this alternative function of LEF1 is independent of WNT/β-catenin signaling.

In conclusion, we identified a new role for LEF1 in the regulation of glutathione metabolism and, thereby, in the metastatic colonization of the brain and, most likely, other organs by breast cancer cells. We also gained preliminary insights into WNT/β-catenin independent functions of LEF/TCF during metastatic colonization and, ultimately, chemotherapy resistance. Finally, cellular redox and detoxification systems might present a novel target to inhibit organ colonization, the clinically decisive step of metastasis.

Acknowledgements

The authors thank Jessica Eggert, Meike Schaffrinski, Doris Gaag and Rudolf Jung for their excellent technical assistance; Julia Bode for her support in establishing the intracranial colonization model; and Torben Ruhwedel for his technical advice regarding electron microscopy. This work was performed in the framework of the Regensburg BrainTumor Center (Zentrum fuer Hirntumoren, ZHT; https://www.ukr.de/zentren/zentrum-fuer-hirntumoren/index.php). This work (design of the study and collection, analysis, and interpretation of data and writing the manuscript) was supported by the German Federal Ministry of Education and Science (BMBF) project MetastaSys in the platform Medical Systems (0316173C), the German Research Foundation projects KFO262 and FOR2127 (PU 355/5-1), the European Union Interreg V program (BY-CZ-118), and the Research Program of the Faculty of Medicine, Georg-August-University Göttingen, Germany.

References

1. Chen MT, Sun HF, Zhao Y, et al. Comparison of patterns and prognosis among distant metastatic breast cancer patients by age groups: a SEER population-based analysis. *Sci Rep* 2017;7:9254.
2. Lockman PR, Mittapalli RK, Taskar KS, et al. Heterogeneous blood-tumor barrier permeability determines drug efficacy in experimental brain metastases of breast cancer. *Clin Cancer Res* 2010;16:5664–78.
3. Baumert BG, Rutten I, Dehing-Oberije C, et al. A pathology-based substrate for target definition in radiosurgery of brain metastases. *Int J Radiat Oncol Biol Phys* 2006;66:187–94.
4. Berghoff AS, Rajky O, Winkler F, et al. Invasion patterns in brain metastases of solid cancers. *Neuro Oncol* 2013;15:1664–72.
5. Neves S, Mazal PR, Wanschitz J, et al. Pseudogliomatous growth pattern of anaplastic small cell carcinomas metastatic to the brain. *Clin Neuropathol* 2001;20:38–42.
6. Siam L, Bleckmann A, Chaung HN, et al. The metastatic infiltration at the metastasis/brain parenchyma-interface is very heterogeneous and has a significant impact on survival in a prospective study. *Oncotarget* 2015;6:29254–67.
7. Yoo H, Kim YZ, Nam BH, et al. Reduced local recurrence of a single brain metastasis through microscopic total resection. *J Neurosurg* 2009;110:730–6.
8. Ferguson SD, Wagner KM, Prabhu SS, et al. Neurosurgical management of brain metastases. *Clin Exp Metastasis* 2017;34:377–89.
9. Nguyen DX, Chiang AC, Zhang XH, et al. WNT/TCF signaling through LEF1 and HOXB9 mediates lung adenocarcinoma metastasis. *Cell* 2009;138:51–62.
10. Bleckmann A, Siam L, Klemm F, et al. Nuclear LEF1/TCF4 correlate with poor prognosis but not with nuclear beta-catenin in cerebral metastasis of lung adenocarcinomas. *Clin Exp Metastasis* 2013;30:471–82.
11. Bos PD, Zhang XH, Nadal C, et al. Genes that mediate breast cancer metastasis to the brain. *Nature* 2009;459:1005–9.
12. Cadigan KM, Waterman ML. TCF/LEFs and Wnt signaling in the nucleus. *Cold Spring Harb Perspect Biol* 2012;4:a011213.
13. Kobayashi W, Ozawa M. The epithelial-mesenchymal transition induced by transcription factor LEF-1 is independent of beta-catenin. *Biochem Biophys Rep* 2018;15:13–8.
14. Santiago L, Daniels G, Wang D, et al. Wnt signaling pathway protein LEF1 in cancer, as a biomarker for prognosis and a target for treatment. *Am J Cancer Res* 2017;7:1389–406.
15. Behrens J, von Kries JP, Kuhl M, et al. Functional interaction of beta-catenin with the transcription factor LEF-1. *Nature* 1996;382:638–42.
16. Klemm F, Bleckmann A, Siam L, et al. Beta-catenin-independent WNT signaling in basal-like breast cancer and brain metastasis. *Carcinogenesis* 2011;32:434–42.
17. Pukrop T, Dehghani F, Chuang HN, et al. Microglia promote colonization of brain tissue by breast cancer cells in a Wnt-dependent way. *Glia* 2010;58:1477–89.
18. Hagemann T, Wilson J, Kulbe H, et al. Macrophages induce invasiveness of epithelial cancer cells via NF-kappa B and JNK. *J Immunol* 2005;175:1197–205.
19. Blazquez R, Wlochowitz D, Wolff A, et al. PI3K: a master regulator of brain metastasis-promoting macrophages/microglia. *Glia* 2018;66:2438–55.
20. Bohnenberger H, Oellerich T, Engelke M, et al. Complex phosphorylation dynamics control the composition of the Syk interactome in B cells. *Eur J Immunol* 2011;41:1550–62.
21. Kulakovskiy IV, Vorontsov IE, Yevshin IS, et al. HOCOMOCO: towards a complete collection of transcription factor binding models for human and mouse via large-scale ChIP-Seq analysis. *Nucleic Acids Res* 2018;46:D252–9.
22. Xuan Z, Zhao F, Wang J, et al. Genome-wide promoter extraction and analysis in human, mouse, and rat. *Genome Biol* 2005;6:R72.
23. Ambrosini G, Groux R, Bucher P. PWMScan: a fast tool for scanning entire genomes with a position-specific weight matrix. *Bioinformatics* 2018;34:2483–4.
24. Xia J, Gill EE, Hancock RE. NetworkAnalyst for statistical, visual and network-based meta-analysis of gene expression data. *Nat Protoc* 2015;10:823–44.
25. Xia J, Benner MJ, Hancock RE. NetworkAnalyst—integrative approaches for protein-protein interaction network analysis and visual exploration. *Nucleic Acids Res* 2014;42:W167–74.
26. Szklarczyk D, Franceschini A, Wyder S, et al. STRING v10: protein-protein interaction networks, integrated over the tree of life. *Nucleic Acids Res* 2015;43:D447–52.
27. Shannon P, Markiel A, Ozier O, et al. Cytoscape: a software environment for integrated models of biomolecular interaction networks. *Genome Res* 2003;13:2498–504.
28. Rietkotter E, Bleckmann A, Bayerlova M, et al. Anti-CSF-1 treatment is effective to prevent carcinoma invasion induced by monocyte-derived cells but scarcely by microglia. *Oncotarget* 2015;6:15482–93.
29. Rietkotter E, Menck K, Bleckmann A, et al. Zoledronic acid inhibits macrophage/microglia-assisted breast cancer cell invasion. *Oncotarget* 2013;4:1449–60.
30. Chuang HN, van Rossum D, Sieger D, et al. Carcinoma cells misuse the host tissue damage response to invade the brain. *Glia* 2013;61:1331–46.
31. Spranger S, Bao R, Gajewski TF. Melanoma-intrinsic beta-catenin signalling prevents anti-tumour immunity. *Nature* 2015;523:231–5.
32. Miller FR, Miller BE, Heppner GH. Characterization of metastatic heterogeneity among subpopulations of a single mouse mammary tumor: heterogeneity in phenotypic stability. *Invasion Metastasis* 1983;3:22–31.
33. Bansal A, Simon MC. Glutathione metabolism in cancer progression and treatment resistance. *J Cell Biol* 2018;217:2291–8.
34. Chambers AF, Naumov GN, Varghese HJ, et al. Critical steps in hematogenous metastasis: an overview. *Surg Oncol Clin N Am* 2001;10:243–55.
35. Obenauf AC, Massague J. Surviving at a distance: organ specific metastasis. *Trends Cancer* 2015;1:76–91.
36. Vanharanta S, Massague J. Origins of metastatic traits. *Cancer Cell* 2013;24:410–21.
37. Semenza GL. Hypoxia-inducible factors: coupling glucose metabolism and redox regulation with induction of the breast cancer stem cell phenotype. *EMBO J* 2017;36:252–9.
38. Schild T, Low V, Blenis J, et al. Unique metabolic adaptations dictate distal organ-specific metastatic colonization. *Cancer Cell* 2018;33:347–54.
39. Fischer GM, Jalali A, Kircher DA, et al. Molecular profiling reveals unique immune and metabolic features of melanoma brain metastases. *Cancer Discov* 2019;9:628–45.
40. Lorger M, Felding-Habermann B. Capturing changes in the brain microenvironment during initial steps of breast cancer brain metastasis. *Am J Pathol* 2010;176:2958–71.
41. Qu Y, Wang J, Ray PS, et al. Thioredoxin-like 2 regulates human cancer cell growth and metastasis via redox homeostasis and NF-kappaB signaling. *J Clin Invest* 2011;121:212–25.
42. Yae T, Tsuchihashi K, Ishimoto T, et al. Alternative splicing of CD44 mRNA by ESRP1 enhances lung colonization of metastatic cancer cell. *Nat Commun* 2012;3:883.
43. Sandieson L, Hwang JT, Kelly GM. Redox regulation of canonical Wnt signaling affects extraembryonic endoderm formation. *Stem Cells Dev* 2014;23:1037–49.
44. Wang S, Gao Y, Song X, et al. Wnt signaling-mediated redox regulation maintains the germ line stem cell differentiation niche. *Elife* 2015;4:e08174.
45. Sciacovelli M, Frezza C. Metabolic reprogramming and epithelial-to-mesenchymal transition in cancer. *FEBS J* 2017;284:3132–44.
46. Zheng X, Carstens JL, Kim J, et al. Epithelial-to-mesenchymal transition is dispensable for metastasis but induces chemoresistance in pancreatic cancer. *Nature* 2015;527:525–30.
47. Fischer KR, Durrans A, Lee S, et al. Epithelial-to-mesenchymal transition is not required for lung metastasis but contributes to chemoresistance. *Nature* 2015;527:472–6.